**Table 9.** Light curve solution. (1) Model parameters of a global fit to all available photometric observations, (2) model parameters of a local fit to observations acquired with the satellite MOST.

| Solution | | (1) | (2) |
|---|---|---|---|
| Element | Unit | Value | |
| **Orbital properties** | | | |
| $P$ | (d) | 7.1467±0.0001 | 7.14467±0.000001 |
| $T_{\rm p}$ | (RJD) | 56224.72426±0.00006 | 56224.72637±0.00018 |
| $a$ | ($R_\odot$) | 25.46[2] | 25.46[2] |
| $q$ | | 0.9448[1] | 0.9448[1] |
| $e$ | | 0.0[1] | 0.00224±0.00014 |
| $i$ | (deg) | 87.5315±0.0028 | 87.7492±0.0014 |
| $\omega$ | (deg) | 90 | 70.07±0.93 |
| **Component properties** | | | |
| Component | | Aa / Ab | Aa / Ab |
| $T_{\rm eff}$ | (K) | 9700[1] / 9459.2±1.7 | 9700[1] / 9463±2.1 |
| $\log g_{\rm [cgs]}$ | | 4.275±0.0000 / 4.3580±0.0000 | 4.329±0.0000 / 4.403±0.0000 |
| $\Omega$ | | 15.5192±0.0039 / 16.6468±0.0048 | 15.9200±0.0018 / 16.8739±0.0020 |
| $R$ | ($R_\odot$) | 1.752±0.0000 / 1.542±0.0000 | 1.727±0.0000 / 1.5333±0.0000 |
| $L_{\rm V}$ | | 0.1545±0.0027 / 0.1157±0.0026 | – / – |
| $L_{\rm B}$ | | 0.1484±0.0035 / 0.1103±0.0037 | – / – |
| $L_{\rm U}$ | | 0.1185±0.0051 / 0.0873±0.0050 | – / – |
| $L_{\rm R}$ | | 0.18±0.15[3] / 0.13±0.14[3] | – / – |
| $L_{\rm M}$ | | 0.1649±0.0023 / 0.1235±0.0022 | 0.16697±0.00021 / 0.12303±0.00021 |
| **Passband luminosity of component B** | | | |
| $L^B_{\rm V}$ | | 0.7299±0.0045 | – |
| $L^B_{\rm B}$ | | 0.7413±0.0059 | – |
| $L^B_{\rm U}$ | | 0.7942±0.0086 | – |
| $L^B_{\rm R}$ | | 0.69±0.24[3] | – |
| $L^B_{\rm M}$ | | 0.7207s±0.0038 | 0.71[1]±0.0001 |

**Notes.**
[1] The parameter was kept fixed.
[2] The semimajor axis was not converged, but it was optimized according to a new value of the inclination.
[3] The high uncertainty is caused by insufficient number of observations in the Johnson R band and their poor phase distribution.

Once the positions of all three components are known, objects representing each component can be placed at these positions. For each object the uniform disk was chosen, because all three components are detached and so only minor departures from the spherical symmetry can be expected. The visibility for such model can be computed analytically with following formula:

$$|V_k(u,v)|^2 = \left| \frac{\sum_{j=1}^{N} L_{j,k} \frac{2J_1(\pi\Theta_j B/\lambda_k)}{\pi\Theta_j B/\lambda_k} e^{-2\pi i(ux_j+vy_j)}}{\sum_{j=1}^{N} L_{j,k}} \right|^2 , \quad (10)$$

where index $j$ denotes a component of the triple system, $k$ the spectral band, $V$ the visibility, $(u,v)$ the spatial frequency, $L$ the luminosity fraction, $B$ the length of the baseline, $\Theta$ the diameter of the uniform disk, $\lambda$ the effective wavelength (the central wavelength of the spectra band), $J_1$ the first-order Bessel function, $(x_j, y_j)$ the Cartesian coordinates of a component computed with the Equation (6), and $N$ the total number of components in the system. The uniform disk diameter $\Theta$ is also a wavelength dependent quantity, so a different radius should be derived for each spectral band. Nonetheless, the dependency is very weak; The difference between the uniform disk radii in the two filters is of the order of $10^{-3}$, i.e. below the accuracy, which one is able to achieve.

The model represented by Equation (10) was fitted to the calibrated squared visibility. The optimal set of parameters was searched by the least squares method, minimizing the following chi-square:

$$\chi^2 = \sum_{k=1}^{N_{\rm F}} \sum_{j=1}^{N_{\rm O}} \left| \frac{V^2_k(u_j,v_j) - V^2_{{\rm MODEL},k}(u_j,v_j)}{\sigma_k(u_j,v_j)} \right|^2 , \quad (11)$$

where $V^2_k$ is the observed squared visibility, $V^2_{{\rm MODEL},k}$ the synthetic squared visibility computed with the Equation (10), $(u,v)$ the spatial frequency, $\sigma$ the standard deviation of the observed squared visibility, $N_{\rm O}$ the total number of observations of the squared visibility and the $N_{\rm F}$ the total number of the spectral bands. Equation (11) was minimized with the Sequential Least Squares method (Kraft 1988) implemented within the SciPy scientific library (jon 2001–).

The phase coverage of the inner and the outer orbits is good enough to allow fitting of all orbital elements. However, some elements are better constrained from the spectroscopy and/or photometry, which are available over much longer time intervals than the spectro-interferometry. Those are the orbital periods of the inner orbit $P_1$ and of the outer orbit $P_2$, the epoch of the primary minimum of the inner orbit $T_{\rm min,1}$, and the epoch of the periastron passage of the outer orbit $T_{\rm p,2}$. Our early attempts to fit the squared visibility with the model have shown that the the error bars on the individual estimates of the calibrated visibility are underestimated. The $\chi^2$ given by Eq. (11) divided by the degrees of freedom was $\chi^2_{\rm R} \gtrsim 10$. Therefore the error bar of the calibrated visibilities was forced to be greater than 0.05. This step reduced the $\chi^2_{\rm R} \approx 1$. The convergence of each parameter

was inspected and the result of each trial was confronted with the results from the analysis of the spectroscopy and the photometry. The results has shown that the majority of properties of orbit 2, can be fitted and agree well with spectroscopy and the photometry as well as with previous analyses. Except the epoch of the periastron $T_{\rm p,2}$ and the orbital period $P_2$, all orbital parameters were fitted. The majority of orbital parameters of orbit 1 were unstable and easily converged to implausible solutions. The only two stable parameters, which converged to a plausible solution were the semimajor axis $a_1$ and the length of the ascending node $\Omega_1$. The diameter of the component B $\theta_{\rm B}$ is stable and can be fitted, diameters of components $\theta_{\rm Aa}$ and $\theta_{\rm Ab}$ converge to too high values and were estimated from the solution of the light curve no. 2, which is presented in Table 9 and the Hipparcos parallax. Even though the semimajor axis of the orbit 1 is stable, we decided to constrain the parametric space further by employing following condition:

$$a_1 = a_2 \left[ \frac{P_2^2}{P_1^2}(1+q_2) \right]^{-\frac{1}{3}} . \qquad (12)$$

This way we take advantage of the semimajor axis of orbit 2 ($a_2$), which is better constrained by our data. The mass ratio of orbit 3 was taken from the fit of the RVs presented in Table 6. The luminosity fractions of the three component were optimized and resulted into values, which were roughly in agreement with the results from the fitting of the synthetic spectra to the disentangled ones. The ratio between components Aa and Ab ($L_{\rm R,Aa}/L_{\rm R,A}$) was oscillating between $\approx 1$ and 3, so at the end these parameters were estimated from the solution presented in Table 8. The interferometric solution is listed in Table 10 and a comparison of the observed and computed squared visibilities is shown in Figure C.1. Two different approaches to estimate the uncertainties of the solution presented in Table 10. The first one was based on the local estimation of the covariance matrix and the second one on a Monte Carlo simulation. The latter also served a test of the robustness of the solution, because all optimized parameters were assigned a uniform a prior probability distribution. Initial parameters for the fitting were randomly drawn from this distribution. Correlations between fitted parameters were studied.

## 6. Discussion

### 6.1. Component C

Spectral lines of the fourth component were detected neither via spectral disentangling nor via the comparison with the synthetic profiles. Therefore we estimated the contribution of component C to the total flux from a black-body model to $\approx 1\%$ in the near infrared. The only spectra at our disposal have lower S/N$\approx$ 50 in the infrared region, so the signal of the faintest component is entirely drown in noise.

- The spectroscopic elements ($K_2$, $e_2$, $T_{\rm periastr.,2}$, $P_2$, $\omega_2$) of orbit 2 are best defined by the modelling of the RVs given in Table 6. The results from the fitting of RVs were confirmed by disentangling (see Table 7). The $\chi^2$ minimized with KOREL is more complex, because it relies also on the shape of the disentangled spectra. Therefore we expect the direct analysis of the measured RVs to be more reliable.
- The periastron epoch $T_{\rm periatr.,1}$ and the period $P_1$ of orbit 1 was obtained with a high precision using the photometry and the direct analysis of the RVs. The photometric solution presented in Table 9 yields the best ephemeris especially thanks to high precision observations from the satellite MOST.
- The eccentricity of orbit 1 is oscillating at the order of $10^{-3}$ due to dynamic interaction between orbits 1 and 2. A non-zero eccentricity was detected only from the analysis of the observations from the satellite MOST. The precision of the measured RVs and the squared visibilities is not sufficient to confirm this.
- The inclination $i_1$ of orbit 1 was only determined from the analysis of the photometry. The parameter was not well-constrained by the measured squared visibility and easily converged to an implausible value.
- The luminosity ratios for all three components were estimated from the spectroscopy, photometry and spectro-interferometry. The modelling of the light curve has shown that the contribution of component C to the total light is completely correlated with the inclination and component radii, i.e. for any given values of the third light, the minimizer only adjusted the values of the inclination and component radii. The luminosity ratios estimated from modelling of the squared visibilities returned similar values as the other methods, but with much higher uncertainty. The modelling of the disentangled spectra with the synthetic ones provided the most precise luminosity fractions.
- The effective temperatures $T_{\rm eff}$ of both components of orbit 1 are probably better estimated via the comparison of the disentangled profiles and the synthetic spectra. These temperatures were estimated using a spectrum covering an interval of 590 Å, containing many spectral lines, whereas the photometrically determined temperatures would rely on four broad-band filters only. A reliable determination of both temperatures of two almost identical stars from photometry only is virtually impossible (Prša & Zwitter 2006). Nonetheless, if the temperatures of components Aa and Ab were both fixed at values from Table 8 the ratio between minima depths was incorrect. Therefore we allowed PHOEBE to optimize also the secondary temperature. Afterwards the secondary temperature sank, but stayed within error bars of the spectroscopic estimate.
- The mass ratio $q_2 = 1.084 \pm 0.006$ of component B and the eclipsing binary, obtained from the analysis of RVs likely has much higher uncertainty than the locally estimated one (see the following section).

At this point each model was re-computed with only those parameters free, which are not better constrained by other measurements and models. A summary of the properties of the triple subsystem based on these final models in Table 11.

### 6.2. Final properties of the system and its components

The sets of parameters defining models which were used throughout this study overlap considerably. As we proceeded through the analyses of the observations based on different methods, we have already used results from one method to constraint the parametric space of another. In some cases it was mandatory, because the solution was degenerated, in other cases it was beneficial, because one of the methods constrained a parameter better. In the following list we justify choice of methods which yield better precision than the remaining ones:

### 6.3. The mass ratio of orbit 2

An attempt to combine the results from the analyses of spectroscopic, photometric and interferometric observations revealed a serious discrepancy. The problem follows:

**Table 10.** Parameters corresponding to the best-fit of the interferometric observations with the model defined by Eqs. (6)–(10).

| Elements | Units | Values | | |
|---|---|---|---|---|
| | | Component properties | | |
| Component | | B | Aa | Ab |
| $\theta$ | (mas) | 0.438±0.004 | 0.251[1] | 0.222[1] |
| $L_{\rm BLUE}$ | | 0.76[1] | 0.13[1] | 0.11[1] |
| $L_{\rm RED}$ | | 0.72[1] | 0.16[1] | 0.12[1] |
| | | Orbital properties | | |
| Orbit | | 2 | | 1 |
| $P_{\rm anomal.}$ | (d) | 145.567[1] | | 7.1467[1] |
| $T_{\rm periastr.}$ | (RJD) | 55609.05[1] | | – |
| $T_{\rm min.I}$ | | – | | 56224.7249[1] |
| $a$ | (mas) | 15.63±0.05 | | 1.63±0.02 |
| $e$ | | 0.215±0.001 | | 0.0[1] |
| $q$ | | – | | 0.96[1] |
| $i$ | (deg) | 86.30±0.04 | | 86.3[1] |
| $\omega$ | (deg) | 7.6±0.2 | | 90.0[1] |
| $\Omega$ | (deg) | 147.87±0.3 | | 325.3±0.3 |
| $k^{\omega}$ | (deg yr$^{-1}$) | 2.74 | | – |

**Notes.**
[1] The parameter was kept fixed.

**Table 11.** Summary of the system based on previous analyses of the spectroscopic, photometric, astrometric and spectro-interferometric observations.

| Parameter | Unit | Value | | |
|---|---|---|---|---|
| | | Component properties | | |
| Component | | B | Aa | Ab |
| $T_{\rm eff}$ | (K) | 13920±460 | 9700±150 | 9580±250 |
| $\log g_{\rm [cgs]}$ | | 4.234±0.080 | 4.275 | 4.3580 |
| $v \sin i$ | (km s$^{-1}$) | 240.6±5.9 | 23.0±1.0 | 20.5±1.2 |
| $M$ | (M$_\odot$) | 3.66[1] | 2.232±0.012 | 2.109±0.011 |
| $R$ | (R$_\odot$) | 3.019±0.028[2] | 1.727±0.001 | 1.5333±0.001 |
| $\theta$ | (mas) | 0.439±0.004 | 0.2541±0.0001[2] | 0.2224±0.0001[2] |
| | | Orbital properties | | |
| Orbit | | 2 | | 1 |
| $P_{\rm anomal.}$ | (d) | 145.567±0.044 | | 7.14665±0.00001 |
| $P_{\rm sid}$ | (d) | 145.125±0.044 | | 7.14665±0.00001 |
| $T_{\rm periastr.}$ | (RJD) | 55609.05±0.48 | | – |
| $T_{\rm min.I}$ | (RJD) | – | | 56224.7243±0.0002 |
| $a$ | (R$_\odot$) | 232.6±1.7 | | 1.847[2] |
| $a$ | (mas) | 15.90±0.01 | | 0.0000±0.0000 |
| $e$ | | 0.2211±0.002 | | 0.0 |
| $i$ | (deg) | 86.81±0.01 | | 87.532±0.003 |
| $\omega$ | (deg) | 187.8±0.5 | | 90.0 |
| $\Omega$ | (deg) | 148.46±0.01 | | 320.2±0.2 |
| $k^{\omega}$ | (deg yr$^{-1}$) | 2.74±0.30 | | 0.0 |

**Notes.**
[1] Estimated assuming orbital inclination $i_2 = 86.81$ deg and the mass ratio $q_2 = 0.85$.
[2] Estimated assuming Hipparcos parallax $\pi = (0.0156 \pm 0.0010)$ mas. The parallax was used to estimate the error bar, because it would dominate it completely.

– If the 3-star solution from Table 6 and the solution (1) of the light curve from Table 9 were accepted, the mass of component B would be $M_{\rm B} = (2.84 \pm 0.04)\,{\rm M}_\odot$ and the total mass of the eclipsing binary $M_{\rm Aa+Ab} = (2.62 \pm 0.03)\,{\rm M}_\odot$.
– If the 3-star solution from Table 6 and the inclination of orbit 2 from analysis of the interferometry were accepted, the inferred mass of component B would be $M_{\rm B} = (4.71 \pm 0.03)\,{\rm M}_\odot$.

Given the temperature of component B (see Table 8), the spectral type of this component is B6-7V star whose mass lies within interval of 3.5 to 3.9 M$_\odot$ (Harmanec 1988). Also the total mass of the eclipsing pair is inconsistent with their spectral type A0V estimated from the spectroscopy. This led us to conclusion that either the inclination or the mass ratio of orbit 2 is not correct.

At first we tested the credibility of the inclination of orbit 2, which was estimated from interferometry. Several large searches

**Table 12.** A comparison of orbital properties of component B obtained from manually and automatically measured RVs.

| Method | | Automatic | Manual |
|---|---|---|---|
| Element | | | |
| $P_{\rm AN}$ | (d) | 145.567 | 145.567 |
| $T_{\rm p}$ | (RJD) | 55609.05 | 55609.05 |
| $K$ | (km s$^{-1}$) | 36.87±0.58 | 39.82±1.25 |
| $e$ | | 0.207±0.017 | 0.217±0.034 |
| $\omega$ | (deg) | 188.3±1.1 | 191.6±2.2 |
| $k^{\omega}$ | (deg yr$^{-1}$) | 2.75 | 2.75 |
| rms | | 2.86 | 6.13 |
| $N$ | | 51 | 51 |

of the parametric space were conducted and their conclusion is that the interferometry is inconsistent with orbital inclination $i_2 \lesssim 80$ deg. This is also supported by the fact that both JN an CH obtained very similar properties of orbit 2, both using their own tools.

Having the inclination verified we focused on the mass ratio $q_2$ of orbit 2 , which is estimated from the ratio of the semi-amplitudes of the RV curves. Assuming that the masses of components Aa and Ab and the inclination $i_2$ are correct, the mass ratio of orbit 2 has to be $q_2 = 0.845$. This would also yield mass of component B $M_{\rm B} = 3.66\,{\rm M}_{\odot}$, which is consistent with the detected spectral type.

The spectral lines of the eclipsing pair are very sharp and they can be measured with precision less than one km s$^{-1}$ (this was verified through a Monte Carlo simulation). Various subsets of the RV measurements on lines of the eclipsing pair were fitted and the results were consistent with the 3-star solution listed in Table 6. Therefore we believe that the resulting elements and especially the semiamplitude $K_{\rm Aa+Ab}$ correspond to the true nature of the triple system.

The component B has very broad and generally shallow lines. Precision of the measurements was roughly three times worse than for the case of lines of eclipsing stars (verified through MC simulation). To check the validity of the RV measurements obtained via automatic procedure (see Section 3) PH measured RVs of both eclipsing stars using a manual method in which a spectral line is compared with its mirrored profile in program SPEFO (Božić et al. 1995; Horn et al. 1996). RVs of the members of the eclipsing binary were measured on the Mg II 4481 Å spectral line and RVs of component B were measured on Mg II 4481 Å an He I 4471 Å spectral lines. A comparison of the manually and automatically measured RVs is shown in Fig 7. Somewhat surprisingly the automatic procedure systematically detects a lower amplitude of RV of component B and consequently leads to lower semi-amplitude of the best-fit model RV curve, while the measurements on sharp lines of the eclipsing pair are almost the same for both methods. Fits to automatically and manually measured RVs of component B are compared in Table 12. The only fitted elements were the eccentricity, the semiamplitude of the RV curve, the longitude of periastron and the systemic velocity. The semiamplitude of the model RV curve is clearly higher for the manual measuring method, while its rms is more than twice larger than for the RV curve obtained for automatically measured. To investigate this issue we tried to measure RVs of component B using not the disentangled spectra, but synthetic spectra given by parameters in Table 8. A model fitted to these measurements was comparable to those listed in Table 12, but its semiamplitude was only $K_{\rm B} = (33.29 \pm 0.66)$ km s$^{-1}$. This shows that the semiampli-

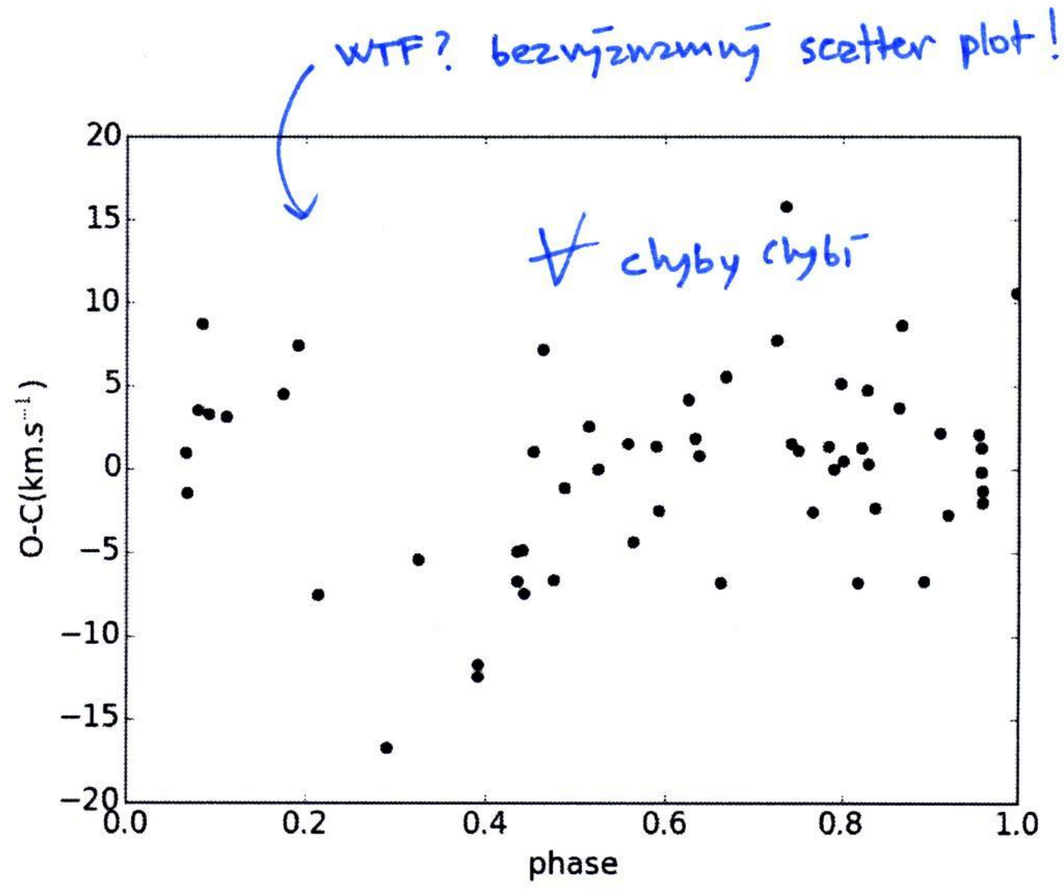


**Fig. 8.** A phase plot of the manually measured residua for orbital period $P_{\rm R} = 0.876$ d and reference epoch $T$=0.0.

tude depends highly on the quality of the chosen template. This may also suggest that this line might be broadened by an additional mechanism, which KOREL is unable to disentangle properly. Nevertheless, even the mass ratio resulting from the analysis of manually measured RVs $q_2^{\rm MANUAL} = 0.945$ still predicts too light components of the eclipsing binary.

The relatively high rms can come from the noise and blends. Especially the He I 4471 Å line blends with several metallic lines and has a pronounced non-LTE component. These two effects make the proper estimation of the position of line wings difficult. It is also possible that our model is not correct and there is an unseen fifth companion. This possibility is explored in the next Section.

The mass ratio of orbit 2 can be also estimated from the astrometric solution. The elements from Table 5 imply total mass of the system $M_{\rm TOTAL} = (8.51 \pm 1.70)$. The error bars, which come mainly from the uncertainty of the parallax are too generous to provide a reliable estimate.

### 6.4. A quintuple "fairy tale"

As already suggested in previous Section, our measurements of RV of component B might be affected by an unseen companion, which causes additional broadening of its spectral lines. The hypothesis is that component B is not a single star, but it is rather a close binary composed of a B-type component and an unseen companion, which distorts the more massive star and that the rapid light variations are actually ellipsoidal variations (see Section 4). The period of the rapid light variations is $P_{\rm R1} = (0.424 \pm 0.005)$ d, so the true orbital period is twice $P_{\rm R} = (0.848 \pm 0.10)$ d.

A search for this period was conducted in residuals of the RV curve fit for both manually and automatically measured RVs. A period of one day was found in residuals of automatically measured RVs, but a period $P_{\rm R} = 0.876$ d was found in residuals of the manually measured RVs. A phase plot of the RV curve is shown in Figure 8. An attempt to fit the radial velocity curve, assuming that the component B is a member of a close binary and semiamplitude of its radial velocity curve is $K_{\rm B} = 44.5$ km s$^{-1}$ returned a model with semiamplitude $K_{\rm R} = (4.7 \pm 1.8)$ km s$^{-1}$. The fit is shown in Figure 9.

Zbytečné porovnávání toho, co by mělo vycházet totožně!



zmenšit

toto by snad mohl být □, ne?

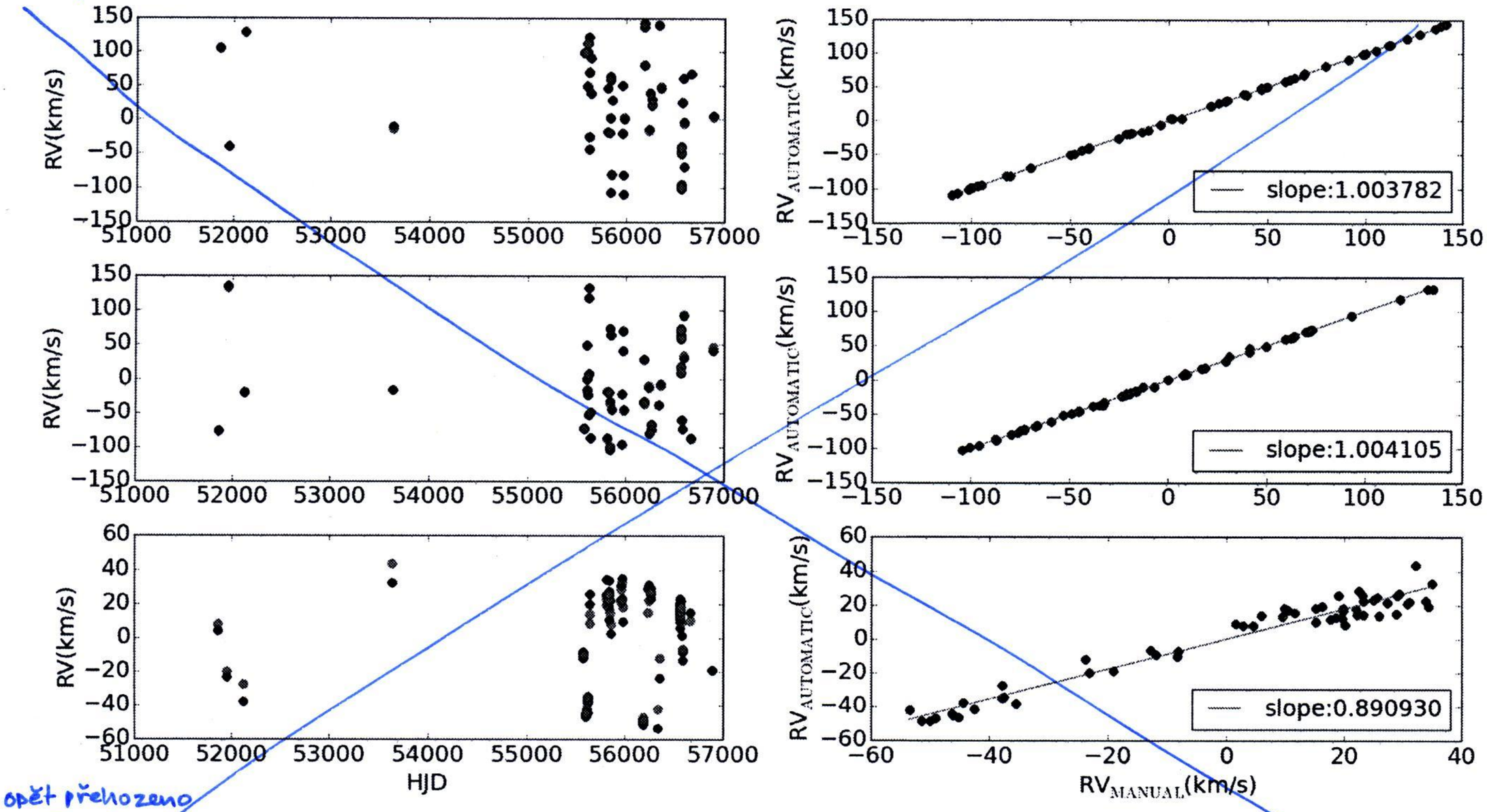


opět přehozeno

**Fig. 7.** Comparison of manually (black) and automatically (red) measured RVs of ξ Tau. The components are following Aa - top panel, Ab - middle panel, B - bottom panel. Left panels - RVs vs. time, right panels - RVs(Manual) vs. RVs(Automatic). The dependency was fitted with a linear function (red line). Its slope is given in the legend.

sepznte sections 7 & 8

### 6.5. Dynamic effects in the system

This section will be done once we accept a final model of component B.

### 6.6. Comparison with models of stellar evolution

This section will be done once we accept a final model of component B.

## 7. Conclusion

*Acknowledgements.* We profited from the use of the program KOREL, written by Dr. P. Hadrava. We acknowledge the use of the publicly available Elodie spectra from the electronic archive of the Haute Provence Observatory. The research of JN, PH, MW, and PZ was supported by the grants P209/10/0715 and GA15-02112S of the Czech Science Foundation. We acknowledge the use of the electronic database from the CDS, Strasbourg and electronic bibliography maintained by the NASA/ADS system.

Following properties of the orbit (denoted with subscript R) can be estimated: (1) The binary orbit is very likely circular due to small distance between the components. (2) The orbital period and the semiamplitude of the 0.876 d orbit imply mass function $f(m)_{\rm R} = 9.42.10^{-6}$. (3) Adopting the primary mass $M_{\rm B} = 3.66\,{\rm M}_{\odot}$ and an inclination one can estimate the mass ratio, the secondary mass and the semimajor axis. A search for an inclination, which would generate ellipsoidal variations comparable to the detected ones was conducted. The model was computed with the program PHOEBE and the inclinations within the interval $I = [15, 30]$ deg generate ellipsoidal variation which agree with the amplitude of the detected rapid light variations (see Section 4). An illustrative comparison for following elements of the rapid orbit is shown in Figure 10: $P_{\rm R} = 0.848$ d, $i_{\rm R} = 20$ deg, $q_{\rm R} = 0.041$, $a_{\rm R} = 6.02\,{\rm R}_{\odot}$, and the secondary mass $M_{\rm Bb} = 0.151$, which would be a late M-type star. Main sequence radii of both stars were assumed and third light coming from the eclipsing binary was also taken into account. It should be pointed out that this hypothesis suffers from a few discrepancies: (1) The best fit solution of the manually-measured RVs of component B yields the semiamplitude $K_{\rm B} = 40\,{\rm km\ s^{-1}}$. The one with $K_{\rm B} = 44.5\,{\rm km\ s^{-1}}$ has $\chi^2$ approximately 20% higher than the former one. Therefore the discrepant mass ratio of orbit 2 cannot be explained by the additional motion of the component B in the 0.876 d orbit. (2) The observed light curve does not indicate any periodical variations of its depth. (3) Fine structure and variations of the period of the light variations are not explained by the model curve. The variations of the orbital motion may arise from tidal interaction of the two components. (4) A simulation which would confirm/disprove stability of such configuration is desirable.

which?

M$_{\odot}$

However,

previous?

Ditto

should be done by us...

## References

2001–, SciPy: Open source scientific tools for Python, [Online; accessed 2015-01-20]
Bolton, C. T. & Grunhut, J. H. 2007, in IAU Symposium, Vol. 240, IAU Symposium, ed. W. I. Hartkopf, P. Harmanec, & E. F. Guinan, 66
Bonneau, D., Clausse, J.-M., Delfosse, X., et al. 2006, A&A, 456, 789
Borkovits, T., Érdi, B., Forgács-Dajka, E., & Kovács, T. 2003, A&A, 398, 1091
Božić, H., Harmanec, P., Horn, J., et al. 1995, A&A, 304, 235
Butterworth, S. 1930, Wireless Engineer, 7
Campbell, W. W. 1909, Astrophysical Journal, 29, 224
Claret, A. 1998, A&AS, 131, 395
Claret, A. 2001, MNRAS, 327, 989
de Laverny, P., Recio-Blanco, A., Worley, C. C., & Plez, B. 2012, A&A, 544, A126

url ?

asi netřeba

váhal bych stavět to ve nejistých základech...

(?) zkusit nějaký model pulzací ?

zvětšit

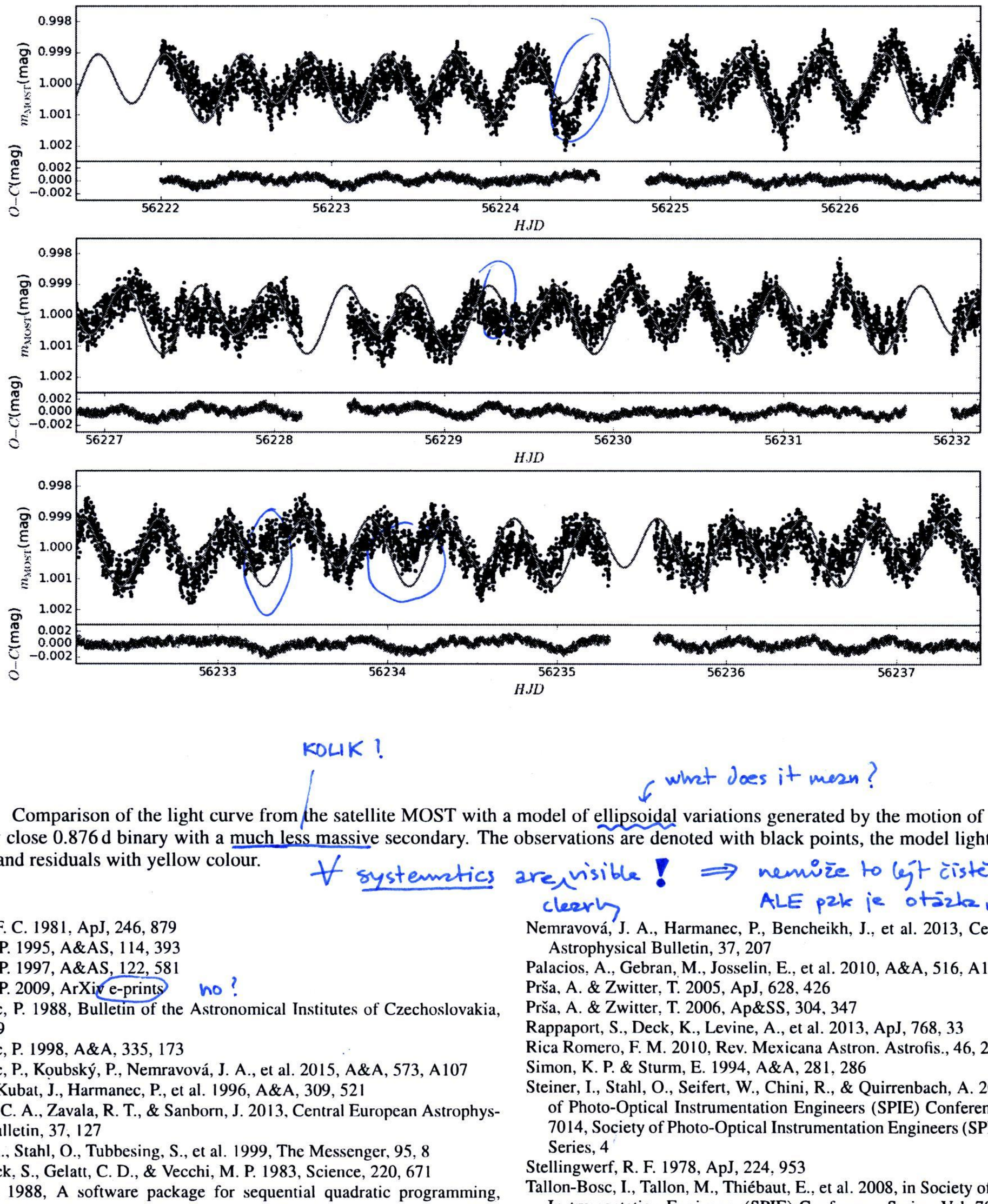


KOLIK ?

what does it mean ?

**Fig. 10.** Comparison of the light curve from the satellite MOST with a model of ellipsoidal variations generated by the motion of component B in a very close 0.876 d binary with a much less massive secondary. The observations are denoted with black points, the model light curve with a red line and residuals with yellow colour.

∀ systematics are clearly visible ! ⇒ nemůže to být čistě geometrický jev, ALE pzk je otázka, zde to nejsou ∀ pulzace


Fekel, J. F. C. 1981, ApJ, 246, 879
Hadrava, P. 1995, A&AS, 114, 393
Hadrava, P. 1997, A&AS, 122, 581
Hadrava, P. 2009, ArXiv e-prints
Harmanec, P. 1988, Bulletin of the Astronomical Institutes of Czechoslovakia, 39, 329
Harmanec, P. 1998, A&A, 335, 173
Harmanec, P., Koubský, P., Nemravová, J. A., et al. 2015, A&A, 573, A107
Horn, J., Kubat, J., Harmanec, P., et al. 1996, A&A, 309, 521
Hummel, C. A., Zavala, R. T., & Sanborn, J. 2013, Central European Astrophysical Bulletin, 37, 127
Kaufer, A., Stahl, O., Tubbesing, S., et al. 1999, The Messenger, 95, 8
Kirkpatrick, S., Gelatt, C. D., & Vecchi, M. P. 1983, Science, 220, 671
Kraft, D. 1988, A software package for sequential quadratic programming, Deutsche Forschungs- und Versuchsanstalt für Luft- und Raumfahrt Köln: Forschungsbericht (Wiss. Berichtswesen d. DFVLR)
Lafrasse, S., Mella, G., Bonneau, D., et al. 2010, VizieR Online Data Catalog, 2300, 0
Lenz, P. & Breger, M. 2004, in IAU Symposium, Vol. 224, The A-Star Puzzle, ed. J. Zverko, J. Žižnovský, S. J. Adelman, & W. W. Weiss, 786–790
Mason, B. D., Martin, C., Hartkopf, W. I., et al. 1999, AJ, 117, 1890
Mason, B. D., Wycoff, G. L., Hartkopf, W. I., Douglass, G. G., & Worley, C. E. 2001, AJ, 122, 3466
Moultaka, J., Ilovaisky, S. A., Prugniel, P., & Soubiran, C. 2004, PASP, 116, 693
Mourard, D., Clausse, J. M., Marcotto, A., et al. 2009, Astronomy and Astrophysics, 508, 1073
Nasseri, A., Chini, R., Harmanec, P., et al. 2014, A&A, 568, A94
Nelder, J. A. & Mead, R. 1965, The Computer Journal, 7, 308
Nemravová, J. A., Harmanec, P., Bencheikh, J., et al. 2013, Central European Astrophysical Bulletin, 37, 207
Palacios, A., Gebran, M., Josselin, E., et al. 2010, A&A, 516, A13
Prša, A. & Zwitter, T. 2005, ApJ, 628, 426
Prša, A. & Zwitter, T. 2006, Ap&SS, 304, 347
Rappaport, S., Deck, K., Levine, A., et al. 2013, ApJ, 768, 33
Rica Romero, F. M. 2010, Rev. Mexicana Astron. Astrofis., 46, 263
Simon, K. P. & Sturm, E. 1994, A&A, 281, 286
Steiner, I., Stahl, O., Seifert, W., Chini, R., & Quirrenbach, A. 2008, in Society of Photo-Optical Instrumentation Engineers (SPIE) Conference Series, Vol. 7014, Society of Photo-Optical Instrumentation Engineers (SPIE) Conference Series, 4
Stellingwerf, R. F. 1978, ApJ, 224, 953
Tallon-Bosc, I., Tallon, M., Thiébaut, E., et al. 2008, in Society of Photo-Optical Instrumentation Engineers (SPIE) Conference Series, Vol. 7013, Society of Photo-Optical Instrumentation Engineers (SPIE) Conference Series
ten Brummelaar, T. A., McAlister, H. A., Ridgway, S. T., et al. 2005, ApJ, 628, 453
Tokovinin, A. A. 1997, A&AS, 124, 75
van Leeuwen, F. 2007, A&A, 474, 653
Walker, G., Matthews, J., Kuschnig, R., et al. 2003, PASP, 115, 1023
Zasche, P., Uhlař, R., Kučáková, H., Svoboda, P., & Mašek, M. 2014, Information Bulletin on Variable Stars, 6114, 1

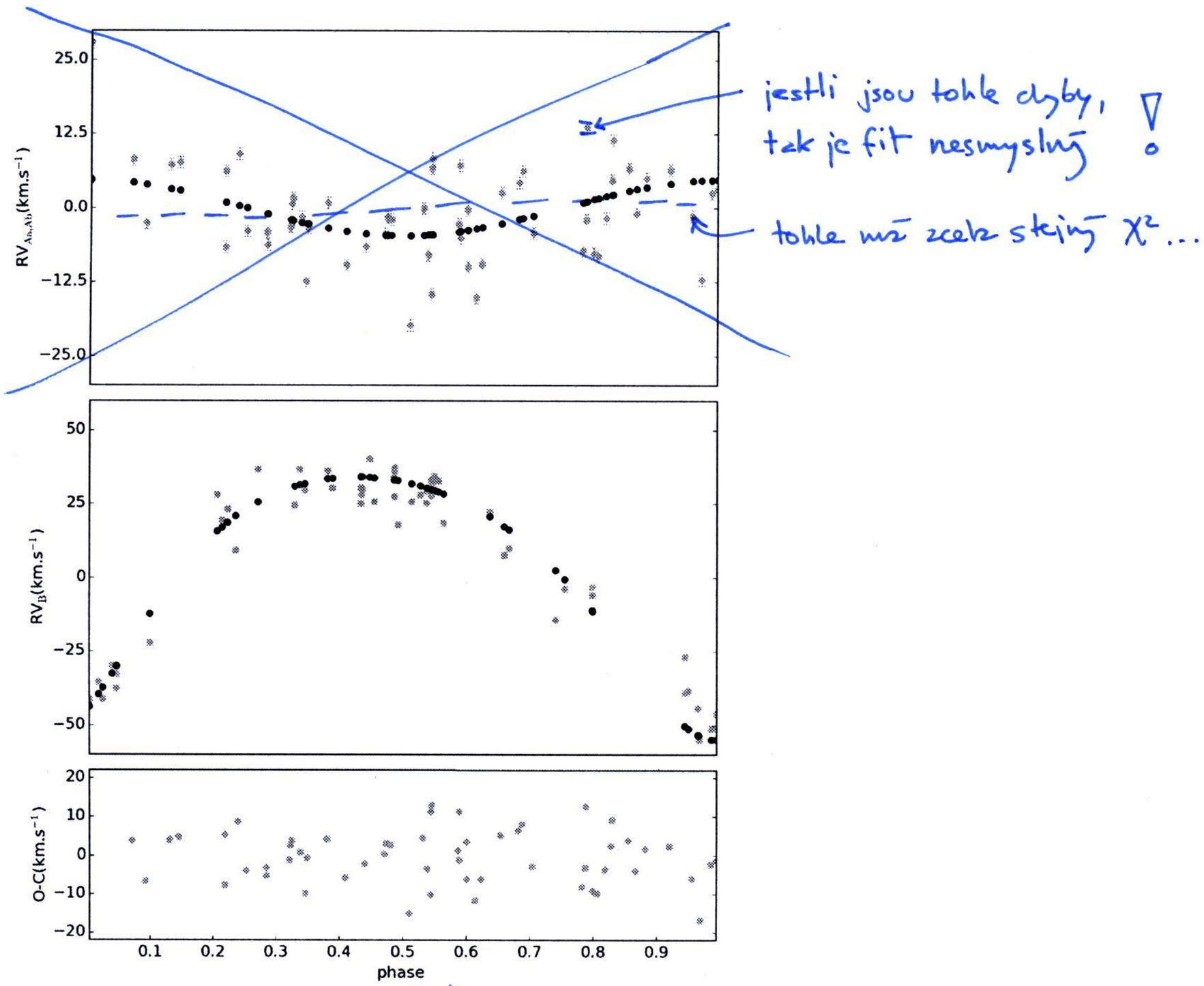


jestli jsou tohle chyby, tak je fit nesmyslný !

tohle má zcela stejný $\chi^2$ ...

**Fig. 9.** A fit to the manually (see 6.4 for details) measured RVs of component B. It is assumed that component B is a member of a close binary. Top panel: the close orbit with period $P_R = 0.876$ d. Middle panel: orbit 2.

what

∀ Bottom panel

∀ different points

## Appendix A: Details on spectroscopic data sets

## Appendix B: Details on photometric data sets

Here, we provide some details on the photometric observations.

- inafter our

## Appendix C: Interferometric fits

nebude to příliš dlouhé?

✗ proč tu není proložen fiwélní model ?

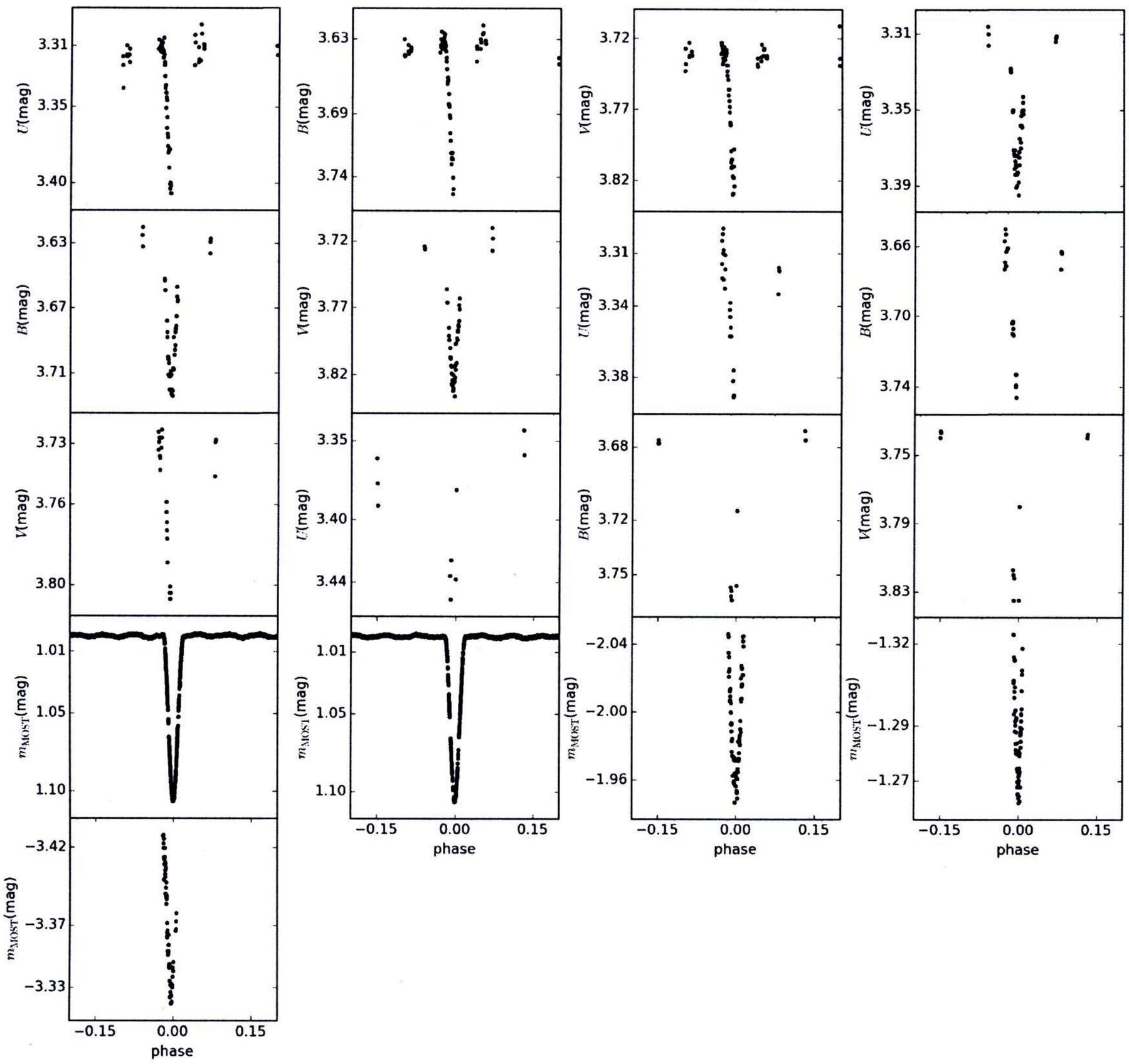


of what ?

**Fig. B.1.** All available primary minima of orbit 1. The filters are denoted as follows: $UBV$ - Johnson's UBV filters, $m_{\rm MOST}$, the filter of the satellite MOST.

přílišs krátké

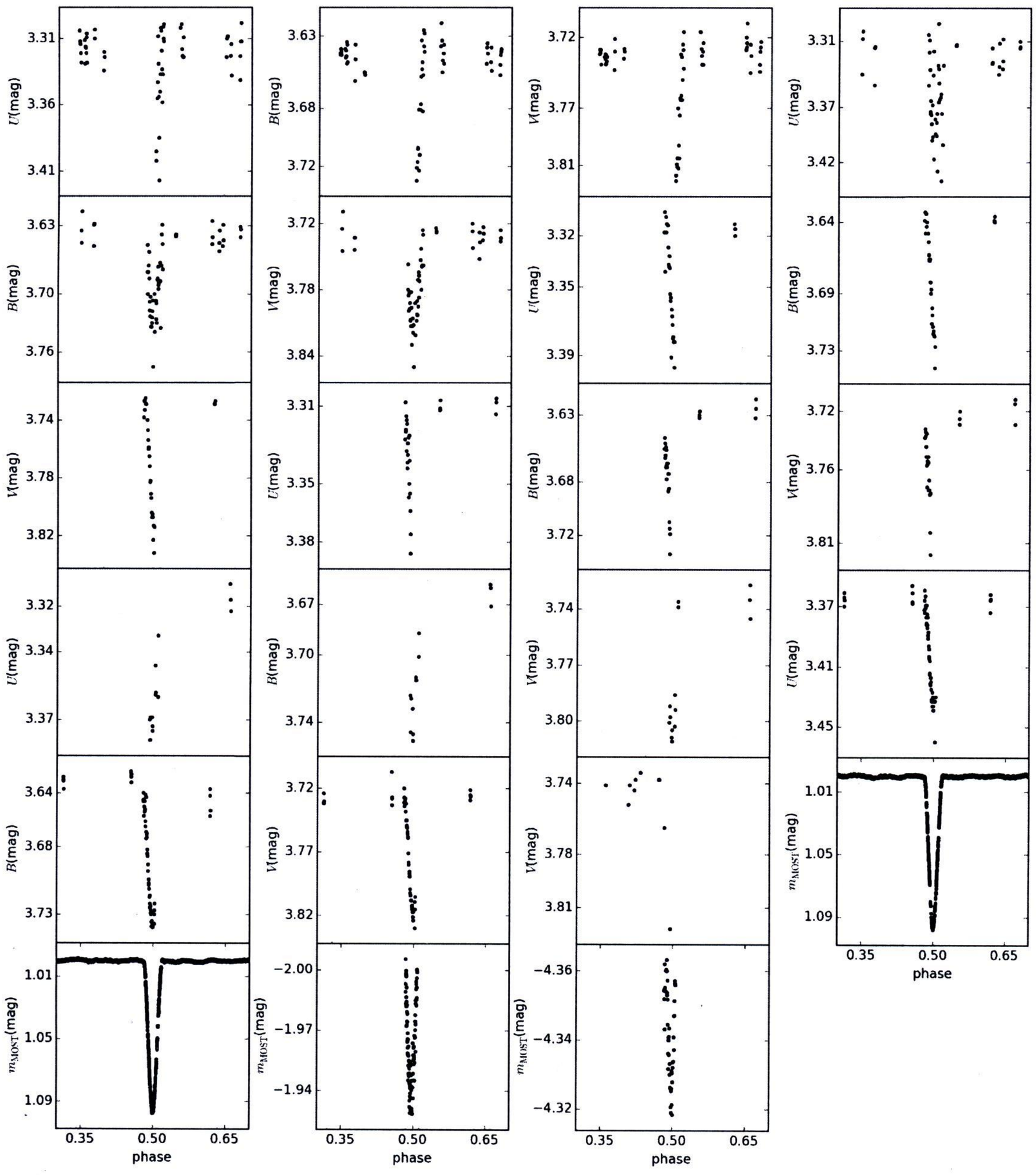


**Fig. B.2.** All available secondary minima of orbit 1. The filters are denoted as follows: $UBV$ - Johnson's UBV filters, $m_{\rm MOST}$, the filter of the satellite MOST.

some of the fits are very poor! ⇒ these will increase $\chi^2$ substancially
are they somehow special?



symboly (zakrývají chyby)

Δ najsou dobře

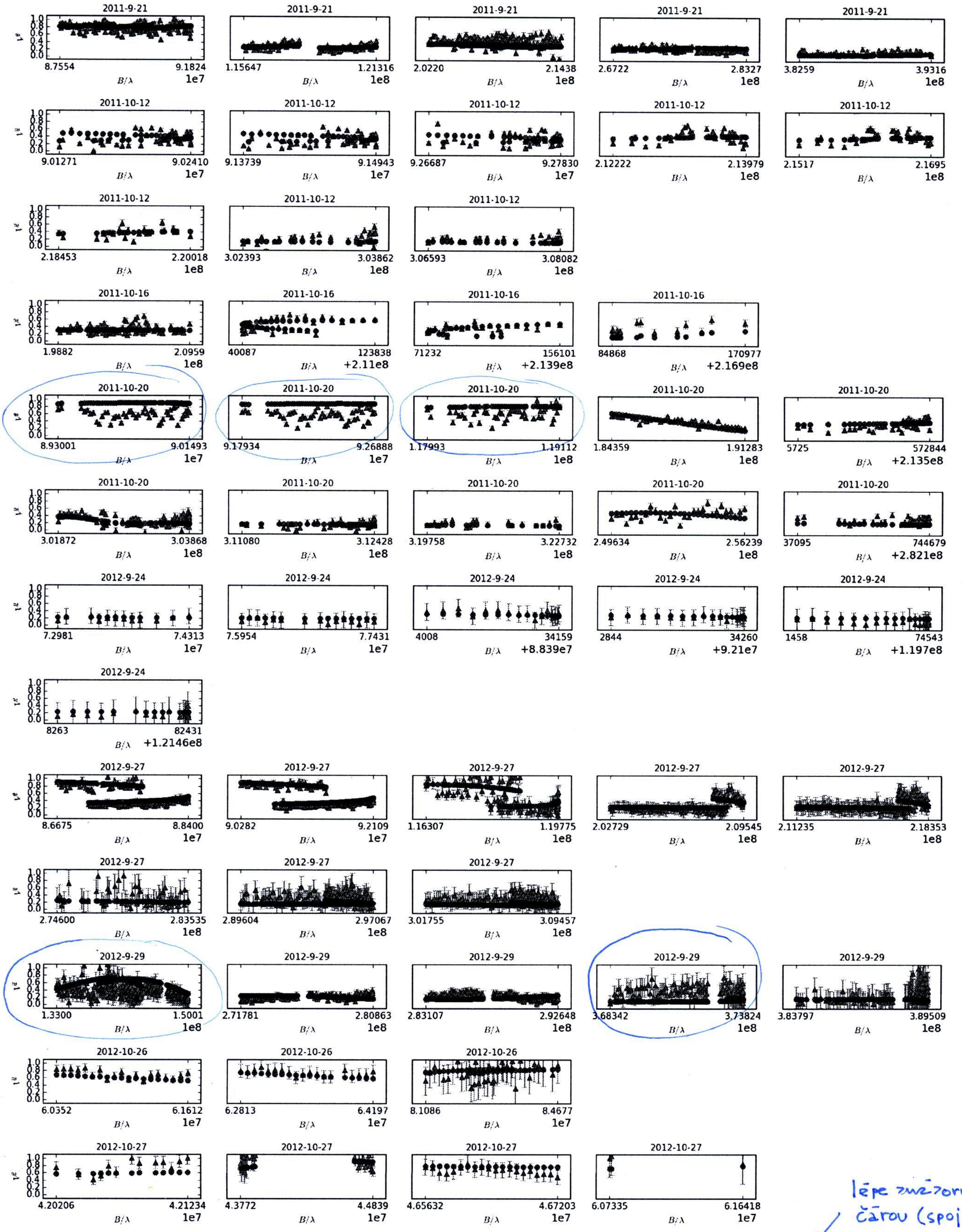


**Fig. C.1.** Fit of the orbital model to the CHARA/VEGA spectro-interferometric observations. Black points denote model defined by Eqs. (6), (10), red points the calibrated squared visibilities. The night during which the data were recorded is given in format YYYY.MM.DD above each panel.

lépe znázornit čárou (spojnicí)!

} dtto

∀ co je na osách